Cleaner Engineering and Technology 5 (2021) 100268

Contents lists available at ScienceDirect

Cleaner Engineering and Technology

journal homepage: www.sciencedirect.com/journal/cleaner-engineering-and-technology

Absorbance determination and photocatalytic production of hydrogen using tungsten and TiO_2 oxide nanostructures As catalyst

Luana Góes Soares [a,*], Maurício de Oliveira Vaz [b], Sérgio Ribeiro Teixeira [b], Annelise Kopp Alves [a]

[a] Universidade Federal do Rio Grande do Sul, Ceramic Materials Laboratory, Av. Osvaldo Aranha 99, sala 705, Porto Alegre, RS, 90035-190, Brazil
[b] Universidade Federal do Rio Grande do Sul, Films and Nanostructures Laboratory, Av. Bento Gonçalves 9500, sala M111, Porto Alegre, RS, 90650-970, Brazil

ARTICLE INFO

Keywords:
Nanostructures
Water splitting
Point defects
Absorbance
Hydrogen

ABSTRACT

In this paper, we described the production of hydrogen using the water splitting method, in which catalytic reactions activate a photocatalyst in the presence of UVA/vis light. This catalyst breaks the water molecule, from which hydrogen is removed. Currently, the substitution of fossil fuels for alternative energy sources is still insufficient. The great advantage of using an alternative energy source such as hydrogen is that in addition to being clean and renewable, it also does not emit carbon-based gases into the atmosphere. To advance the use of hydrogen, we synthesized TiO_2 and TiO_2 nanostructures mixed with two tungsten precursors (H_2WO_4 and $Na_2WO_4.2H_2O$), aiming to increase the radiation absorption capacity of TiO_2. Synthesized nanostructures were used as photocatalysts for hydrogen production by water splitting. The synthesized materials were analyzed using X-ray diffraction (XRD), scanning electron microscopy (SEM), and absorbance tests performed with a Konica-Minolta spectrophotometer. The $TiO_2/Na_2WO_4.2H_2O$ (800 °C) nanostructures absorbed light in a wider range of wavelengths, and were consequently more efficient in producing H_2. The results show that $Na_2WO_4.2H_2O$ plays an important role in the photoactivity of synthesized materials, as it increases the concentration of point defects in TiO_2 networks, enhancing hydrogen production and the absorption range. The TiO_2, TiO_2/WO_3, and $TiO_2/Na_2WO_4.2H_2O$ catalysts showed the best photocatalytic performance for hydrogen production: 33.5%, 61.6%, and 76.6%, respectively. These samples were synthesized at 800 °C and had specific surface areas of 9.8, 28.5, and 30.9 m^2/g, respectively.

1. Introduction

The use of fossil fuels to generate energy is causing climate change and altering the living conditions of the world population, yet it is not a recent event. These changes began with the increasing technological innovations from the second half of the 18th century, which intensified industrial production and consequently the emissions of polluting gases, such as carbon dioxide (CO_2) and methane (CH_4) (Rifkin, 2003).

This factor, coupled with growing oil prices and global energy demand, and declining reserves of fossil energy sources, has driven developing countries such as Brazil to look for alternative sources of energy (Rifkin, 2003).

Using renewable sources is an opportunity to obtain clean energy and reduce environmental impacts. Thus, hydrogen (H_2) has been considered a good energy source option, as it can be stored for later consumption, be converted into electricity, plus other possible uses. It also serves as a link between different energy forms due to its high energy value (Marques et al., 2017).

Different methods use water splitting – which involves the catalytic reforming of organic compounds and biological processes – to obtain hydrogen. These methods extract hydrogen by breaking down the water molecule (Tolmasquim, 2003), (Hao et al., 2018), (Vasconcelos de Sá et al., 2014).

Hydrogen production can be carried out using:

- primary sources of energy such as coal, oil, and natural gas;
- chemical intermediates such as refinery, ammonia, and ethanol;
- alternative energy sources such as biomass, biogas, and waste gas.

Fig. 1a–b show the energy matrix data regarding the world and Brazil, respectively, according to information from the Energy Research Company (EPE). The text's highlighted parts represent the percentage of

* Corresponding author.
E-mail address: luana.goes@ufrgs.br (L.G. Soares).

https://doi.org/10.1016/j.clet.2021.100268
Received 21 November 2020; Received in revised form 30 August 2021; Accepted 30 August 2021
Available online 1 September 2021

renewable energy used in the world and Brazil, respectively.

As shown in Fig. 1a, the world's energy matrix is based primarily on non-renewable sources such as coal, oil, and natural gas. The use of renewable sources in the world is not yet representative, amounting to only 4.1% of its energy matrix. If we add biomass, renewables comprise 14% of the total energy. In Brazil, renewable sources are widespread, although Brazilian energy consumption is mostly based on non-renewable sources. We employ more renewable sources in power generation than anywhere else in the world: approximately 43% of our matrix, which represents half of the country's energy generation. According to graph 1b, these sources are firewood and charcoal, hydropower, cane derivatives, and other renewable sources (Empresa de Pesquisa Energética, 2020).

Thus, the present study is inserted in this context, as already mentioned. The generation of energy using hydrogen, besides being attractive due to its high energy per unit of mass, also diminishes oil dependence and, consequently, the emission of polluting gases into the atmosphere (El-Yazeed and Ahmed, 2019). As generating energy through catalytic reactions is feasible, we use the heterogeneous photocatalysis method to produce hydrogen, which consists of activating a semiconductor when the material is irradiated with UVA/vis illumination (El-Yazeed and Ahmed, 2019).

Since TiO_2 absorbs only light in the UVA region, due to its broad bandgap (3.2 eV) (Marques et al., 2017) and (Tan et al., 2018), some alternatives have been created to extend its absorption range doping or mixing with other metals. Using the electrospinning method, we have developed photocatalytic TiO_2 and TiO_2 nanostructures containing tungstic acid (H_2WO_4) or sodium tungstate dihydrate ($Na_2WO_4.2H_2O$). The results indicate that the presence of spot defects (waves in oxygen, hydroxyl group, and sodium atoms) in the synthesized nanostructures increases the visible light absorbance of the samples and their photocatalytic hydrogen production.

2. Experimental

2.1. Chemicals and materials

TiO_2, TiO_2/WO_3, and $TiO_2/Na_2WO_4.2H_2O$ fibers (catalysts) were obtained by electrospinning following the preparation of solutions containing the precursors: titanium propoxide (Sigma-Aldrich), glacial acetic acid (Neon), polyvinylpyrrolidone (Sigma-Aldrich), anhydrous ethyl alcohol (Zeppelin), tungstic acid (Sigma-Aldrich), sodium tungstate dihydrate (Dynamics), hydrogen peroxide (Sigma-Aldrich), and the TiO_2–P25 (Evonik) as a reference standard.

2.1.1. Electrospinning

The electrospinning method was used to synthesize the catalysts. Firstly, 4 types of precursor solutions ware produced, containing TiO_2–P25 or, titanium propoxide for TiO_2 catalysts; or titanium propoxide and tungstic acid for TiO_2/WO_3 catalysts; or titanium propoxide and sodium tungstate dihydrate for $TiO_2/Na_2WO_4.2H_2O$ catalysts.

In summary, 5 mL of each of the four solutions were transferred to a plastic syringe. The syringe was connected to a stainless-steel hypodermic needle and attached to a high voltage source. The distance between the needle tip and the cylindrical collector (coated with an aluminum foil) was 12 cm; the working voltage was 13.5 kV, and the flow of the precursor solution was 1.8 mL/h. The produced catalysts were collected every 30 min for 4 h. Heat treatment was performed from 650 °C up to 800 °C in an electric oven (SANCHIS) using a heating rate of 1.4 °C/min for 1 h.

2.1.2. Characterization nanostructures

An X-ray diffractometer (Phillips, MDP) using CuKα radiation and a voltage of 40 kV and 40 mA was used to collect the data for phase identification. A scanning electron microscope (SEM, JEOL JSM 6060 equipped with an EDS spectrophotometer) was used to assess catalysts morphology and identify the amounts of Na, W, Ti, and O atoms in the sample, depending on the composition of the precursors. A UV–Vis–NIR (Cary 5000) double-beam spectrophotometer was used to determine the samples' bandgap using the Kubelka-Munk correlation with TAUC

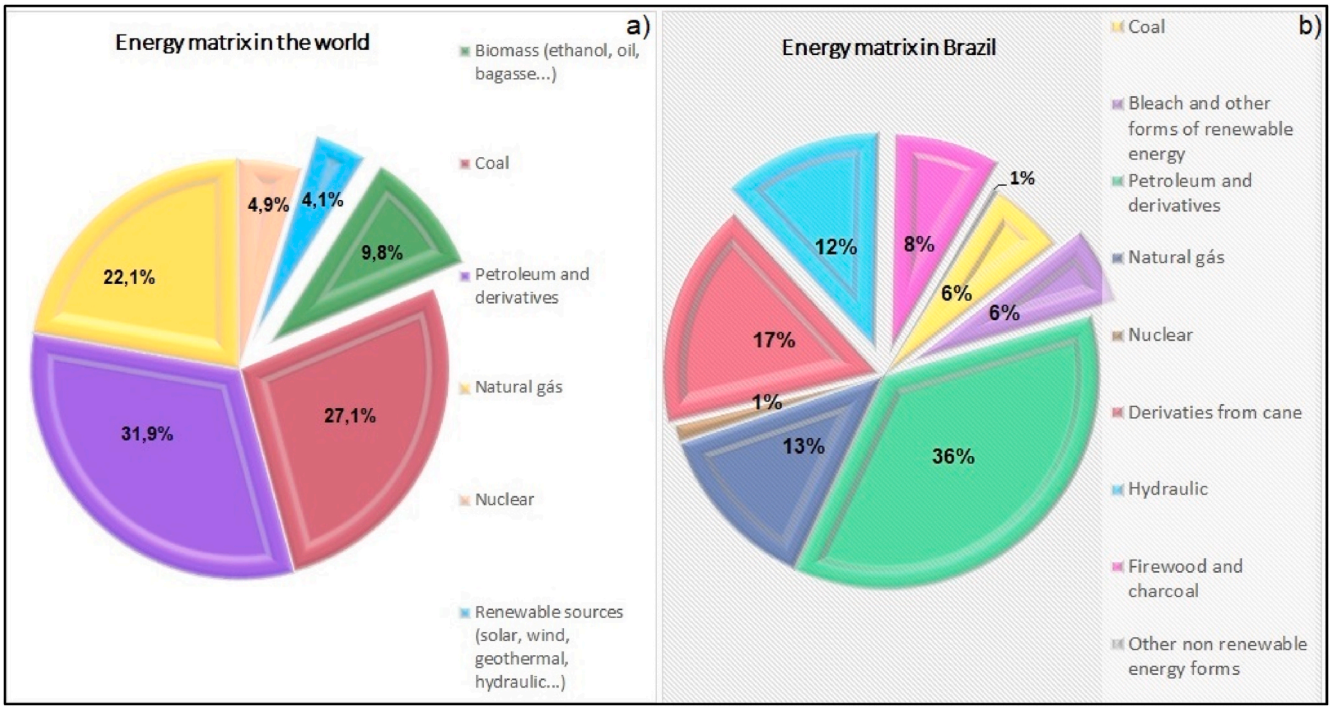

Fig. 1. Graphs showing the (a) energy matrices in the world and (b) in Brazil.

correction. The absorbance curves were analyzed using a Konica-Minolta spectrophotometer CM 2600 d, with an integrated sphere and ultraviolet filter. The specific surface area was measured using the Brunauer Emmett and Teller (BET) method and the Quantachrome instruments Autosorb and Nova 1000e.

2.2. Hydrogen production

For the photocatalytic production of hydrogen, a quartz reactor consisting of double walls through which the water circulated was used, with a constant temperature of 25 °C. Then the catalysts, one at a time, were submerged in a solution of 7.5 mL of deionized water and 2.5 mL of ethanol. Before irradiation began, analytical argon was bubbled to remove the dissolved gases and the system was deaerated through a vacuum airline. A 300 W xenon lamp then illuminated the reactor to simulate sunlight. The produced gases were collected using a Hamilton gas syringe at 30 min intervals for 4 h and quantified using a GC-Agilent 6820 chromatograph. The total volume of the samples injected into the chromatograph was 1.000 μL.

3. Results and discussion

Fig. 2 (a–c) shows the diffractograms of the fibers. The samples without heat treatment (WHT) were amorphous in all formulations. The TiO_2 catalysts formed anatase (JCPDS 01-078-2486) up to 700 °C. From 750 °C, rutile (JCPDS 01-077-0442) was also identified. The TiO_2/WO_3 catalysts treated up to 650 °C, anatase, and brookite (JCPDS 01-075-1582) phases were identified. For WO_3 samples, the monoclinic phase (JCPDS 00-032-1393) was detected at all heat treatment temperatures. The catalysts that were treated at 700 °C showed, in addition to the phases mentioned above, the rutile phase. The $TiO_2/Na_2WO_4.2H_2O$ catalysts had the monoclinic phase of WO_3 and the anatase phase of TiO_2 when treated at 650 °C. For the calcined catalysts at 700 and 750 °C, the anatase and brookite phases of TiO_2 and orthorhombic phases of WO_3 were identified. However, the samples calcined at 800 °C showed, besides the above phases, the rutile and tetragonal phases (JCPDS 00-002-0414) of WO_3 and NaOH (JCPDS 00-035-1009) (Soares and Alves, 2018).

Fig. 3 (a–c) shows SEM images of the sample's morphologies. Generally, all catalysts had a similar microstructure. The TiO_2 samples' surface is composed of fibers without a preferential orientation, thus showing a more elongated microstructure than TiO_2/WO_3, which has a nanorod-like structure with an irregular surface containing WO_3 agglomerates. The $TiO_2/Na_2WO_4{\cdot}2H_2O$ samples contain an agglomerate of elongated fibers with rough surfaces, which can be attributed to the presence of tungsten (Nguyen et al., 2011).

Table 1 shows the bandgap, percentage of tungsten, wavelength, and surface area values of all synthesized samples. One of the strategies for extending the light absorption range to the visible region of TiO_2 is to dope it with other compounds or transition metals. The TiO_2 bandgap is reduced with doping, enabling it – when irradiated with light (solar or artificial) – to break the water molecule, from which hydrogen is extracted for energy production. The processes of absorption and emission of light occur via the transformation of energy, in the form of photons or phonons (Oliveira, 2016). In heterogeneous photocatalysis, the semiconductor needs to have energy equal to or greater than the bandgap to provide the electron with the energy necessary to overcome the semiconductor's bandgap. Simultaneously, electronic holes (h+) are created in the valence band, and the electrons occupy the conduction band, forming electron/hole pairs, which perform water redox reactions. It is worth mentioning that a promising photocatalyst needs to have specific characteristics such as favorable bandgap energy position, good chemical stability, and high surface area.

In general, as can be seen in Table 1, all samples had band gap values that fit the above requirements, allowing the synthesized catalysts to have a good photocatalytic performance when producing hydrogen. Comparing the tungsten-free TiO_2 samples with the tungsten-doped precursor samples (H_2WO_4 and $Na_2WO_4.2H_2O$), it is clear that the addition of these precursors reduces the bandgap, thus increasing light absorption at longer wavelengths. The samples' surface area decreased as the temperature in the heat treatment increased. It was expected because the rise in temperature removes the polyvinylpyrrolidone and other organic compounds from the samples' surface. Despite this reduction, the samples containing H_2WO_4 and $Na_2WO_4.2H_2O$ showed

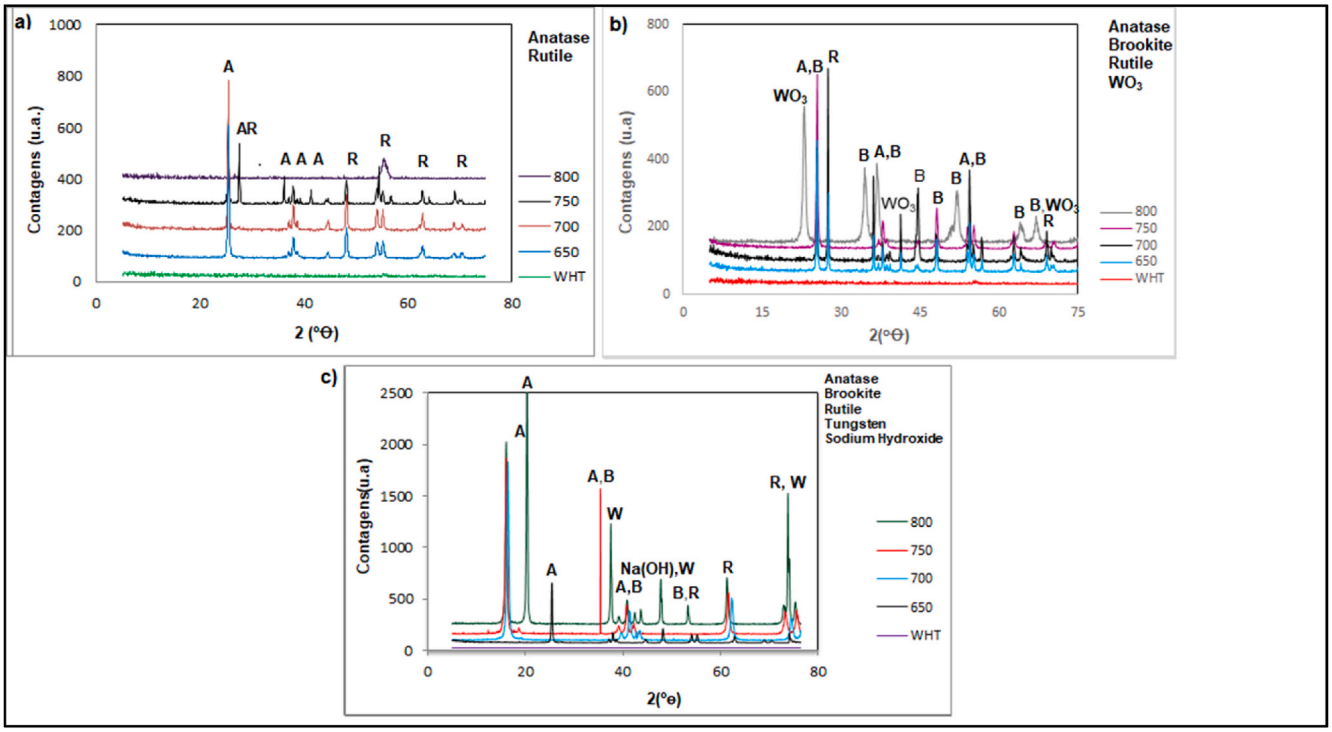

Fig. 2. X-ray diffractogram pattern of (a) TiO_2, (b) TiO_2/WO_3 and (c) $TiO_2/Na_2WO_4.2H_2O$ samples.

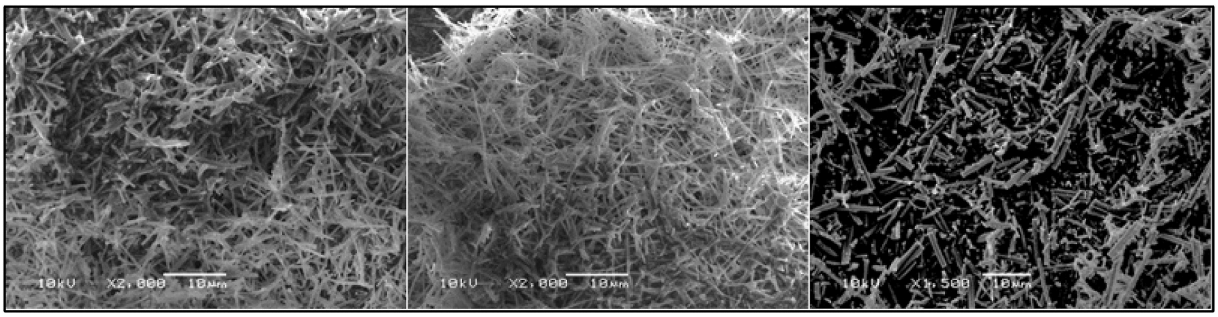

Fig. 3. SEM images and EDS analysis of the (a) TiO_2, (b) TiO_2/WO_3 and (c) $TiO_2/Na_2WO_4.2H_2O$ sample.

Table 1
Bandgap energies, percentages of tungsten, surface areas, and their respective wavelengths (nm).

Samples	Parameters			
	Percentage of W (%)	λ (nm)	Band gap (Ev)	SSA (m^2/g)
Catalysts TiO_2 650 °C	–	382	3.24	32.2
Catalysts TiO_2 700 °C	–	423	2.93	27.5
Catalysts TiO_2 750 °C	–	435	2.85	19.0
Catalysts TiO_2 800 °C	–	439	2.82	9.8
Catalysts TiO_2/WO_3 650 °C	2	480	2.58	60.4
Catalysts TiO_2/WO_3 700 °C	2	482	2.57	41.9
Catalysts TiO_2/WO_3 750 °C	2	484	2.56	36.5
Catalysts TiO_2/WO_3 800 °C	3.1	488	2.54	28.5
Catalysts $TiO_2/Na_2WO_4.2H_2O$ 650 °C	2.2	492	2.52	132.8
Catalysts $TiO_2/Na_2WO_4.2H_2O$ 700 °C	2.21	534	2.32	88.4
Catalysts $TiO_2/Na_2WO_4.2H_2O$ 750 °C	3	546	2.27	33.9
Catalysts $TiO_2/Na_2WO_4.2H_2O$ 800 °C	6.9	553	2.24	30.9
Catalysts TiO_2 P25 Evonik (reference)	–	387	3.2	50.0

large surface areas, giving them a better photocatalytic response.

Fig. 4 shows the absorbance curves of the TiO_2–P25 (reference); TiO_2; TiO_2/WO_3, and $TiO_2/Na_2WO_4.2H_2O$ catalysts in the visible region. As all synthesized samples could absorb visible light (Table 1), we selected one sample from each catalysts composition for explanation purposes. The TiO_2 samples and TiO_2–P25 had maximum absorption at 420 nm. The TiO_2/WO_3 and $TiO_2/Na_2WO_4.2H_2O$ samples showed maximum absorbance at 440 nm and 460 nm, respectively. The absorption of visible light in different regions of the visible spectrum can be related to the samples' bandgap values. A sample can absorb light in

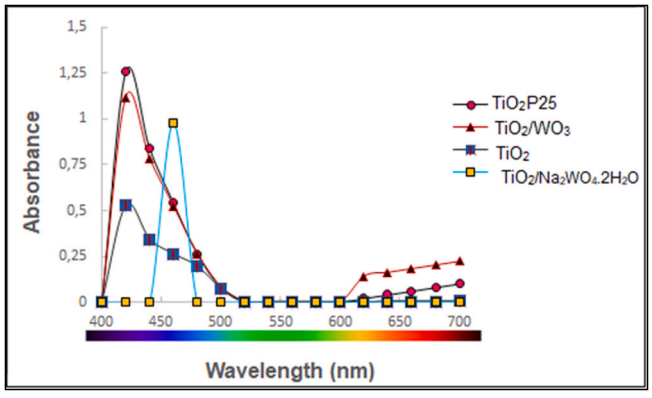

Fig. 4. Absorbance curves of TiO_2–P25 (reference), TiO_2, TiO_2/WO_3, and $TiO_2/Na_2WO_4.2H_2O$ catalysts during irradiation using visible light.

longer wavelengths with a smaller bandgap, as was demonstrated by the $TiO_2/Na_2WO_4.2H_2O$ samples, which at 800 °C had a bandgap value of 2.24 eV and absorbed light at 553 nm. We also highlight the formation of point defects (oxygen vacancies), which occur to a greater or lesser extent in all crystalline materials. The high concentration of these defects in the samples provide the electrons greater mobility within the material. This movement is acquired when the valence electrons, i.e., those responsible for binding atoms, are excited at higher energy levels. Such excitation generates an electron in the conduction band and a gap in the materials' valence band Muccillo in 2008, described and compared the main characteristics related to the transport properties of some oxygen ion conductors. Garcia et al., In 2018, reported in their study the synthesis by the oxidizing peroxide method and microwave-assisted hydrothermal treatment of titanium dioxide nanostructures with good properties and high photocatalytic activity. Finally, Kingery wrote in 1976 about the properties of crystals and how they are determined by imperfections or specific defects.

Fig. 5 (a–c) shows the evolution of hydrogen gas production by the TiO_2–P25 (reference), TiO_2, TiO_2/WO_3, and $TiO_2/Na_2WO_4.2H_2O$ catalysts. All synthesized samples produced hydrogen. The highest H_2 production were achieve by the catalysts containing tungsten precursors (TiO_2/WO_3 – 800 °C, 61.6% and $TiO_2/Na_2WO_4.2H_2O$ – 800 °C, 76.6%), as shown in Table 2. Results obtained by the aid X-ray diffraction (XRD) and Energy Dispersive Spectroscopy (EDS) analyses, which identified the percentage of tungsten in the fiber (catalysts) containing these precursors, indicated 3.1% and 6.9% tungsten in their structures, respectively (Table 1). These results confirmed that the inclusion of this element, associated with the increase of the heat treatment temperature and the bandgap reduction, contributed to the formation of a larger number of oxygen vacancies. According to the literature (Muccillo, 2008) conduction occurs through consecutive leaps of oxygen ions in the vacancies within the TiO_2 crystal structure in almost all oxygen ion conductors. The joint action of these factors gave titanium structural phase stability. Rising heat treatment temperatures allowed O_2 vacancies to acquire the mobility required to move in a disordered state inside the anionic subnet (Muccillo, 2008), (Miyazawa et al., 2018) and (Bharti et al., 2016). The OH group on the surface of $TiO_2/Na_2WO_4.2H_2O$ catalysts replaced the oxide in the TiO_2 substrate, causing vacancies to form a bridge between titanium bonds (Body et al., 2017), contributing to the electron transfer between the two semiconductors and decreasing the chances of recombination between the electron/hole pair (Prabhu et al., 2014), (Patsoura et al., 2006), and (Patsoura et al., 2007). Sato and White, in 1980, also found that hydrogen production using TiO_2 is not caused by the breakdown of the water molecule via photocatalysis but occurs due to the photo-assisted oxidation that takes place in reduced TiO_2 oxygen vacancies.

Table 2 shows, in terms of values, how much hydrogen each sample produced. The TiO_2, TiO_2/WO_3 and $TiO_2/Na_2WO_4.2H_2O$ catalysts that showed the best photocatalytic performance for hydrogen production. The TiO_2, TiO_2/WO_3, and $TiO_2/Na_2WO_4.2H_2O$ catalysts showed the best photocatalytic performance for hydrogen production: 33.5%, 61.6%,

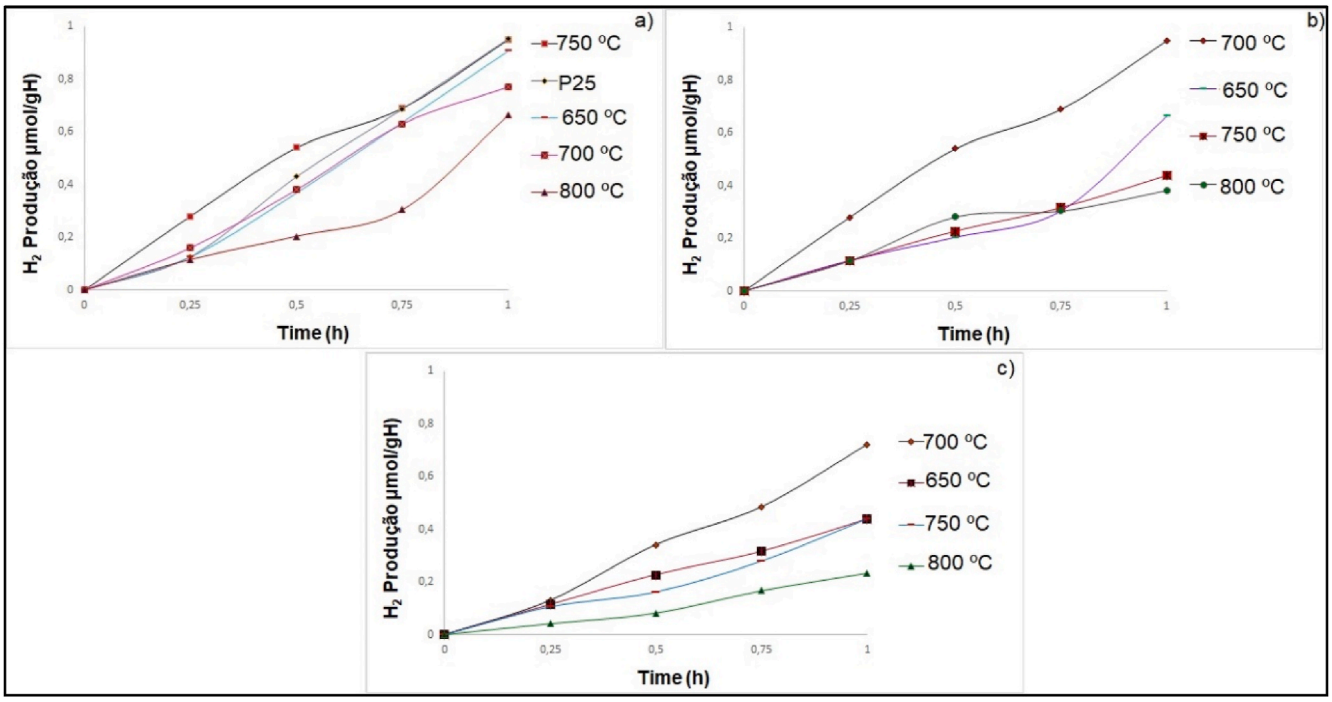

Fig. 5. Photocatalytic hydrogen production using synthesized sample as catalysts.

Table 2
Shows, in terms of values, how much hydrogen each sample.

Samples	Parameter
	H_2 Production (%)
Catalysts TiO_2 650 °C	9.12%
Catalysts TiO_2 700 °C	23%
Catalysts TiO_2 750 °C	4.58%
Catalysts TiO_2 800 °C	33.51%
Catalysts TiO_2/WO_3 650 °C	35.42%
Catalysts TiO_2/WO_3 700 °C	5%
Catalysts TiO_2/WO_3 750 °C	56.31%
Catalysts TiO_2/WO_3 800 °C	61.65%
Catalysts $TiO_2/Na_2WO_4.2H_2O$ 650 °C	27.96%
Catalysts $TiO_2/Na_2WO_4.2H_2O$ 700 °C	56.08%
Catalysts $TiO_2/Na_2WO_4.2H_2O$ 750 °C	56.32%
Catalysts $TiO_2/Na_2WO_4.2H_2O$ 800 °C	76.63%
Catalysts TiO_2 P25 Evonik (reference)	4.56%

and 76.6%, respectively. These samples were synthesized at 800 °C and had specific surface areas of 9.8, 28.5, and 30.9 m^2/g, respectively (Table 1). The larger specific surface area can also explain the fact that the $TiO_2/Na_2WO_4.2H_2O$ sample heat treated at 800 °C was the most photoactive during hydrogen production, besides the presence of Na^+ ions, which also contributed to the increase of hydroxyl groups (OH) on the surface of the material. (El-Yazeed and Ahmed, 2019), report in their study the synthesis of mesoporous WO_3/TiO_2 photocatalysts, with different weight loads of WO_3, which were used in the removal of an aqueous solution of methylene blue. The FTIR results showed that the OH groups bound more easily to the sample surface 10% by weight of WO_3/TiO_2, which influenced the increase in its photodegradation capacity in the UV–visible region. (Sato and White, 1980), describe in their work the photocatalytic decomposition of water, using powdered Pt/TiO_2 as semiconductor, when irradiated with UV light. (Li et al., 2017), investigated in detail the chemical composition of $TiOF_2$, and revealed the influence of the presence of OH groups in the $TiOF_2$ sub-network, which induce the formation of titanium vacancies. And, (Chou et al., 2012), report that a tungsten oxide photoanode, prepared by atomic layer deposition, can be stabilized by a compound Mn-oxo, producing oxygen and hydrogen by water-splitting. Already (Liu et al., 2011) produced by atomic layer deposition of WO_3 and stabilized with an oxygen evolution catalyst based on Mn. The resulting electrode absorbs photons to create electrons and holes, the separation of which is aided by the field embedded within the semiconductor. Electrons are collected and holes transferred to the catalyst to split H_2O into oxygen and hydrogen.

4. Conclusions

This study showed that electrospinning methods are a practical pathway for synthesizing tungsten doped TiO_2 catalysts. All prepared samples showed photocatalytic activity for hydrogen production. Microstructural investigations revealed that the synthesis processes did not affect the phases or morphology of the samples. Among all the synthesized samples, TiO_2 catalysts at 750 °C had the lowest hydrogen production capacity (4.5%), probably because TiO_2 in pure water have a higher electron/hole pair recombination speed, which results in the termination of the photocatalytic effect after a short period of exposure to light. We produced H_2 using TiO_2 sample by applying ethanol molecules as sacrificial reagents, which functioned as electron donors for hydrogen photogeneration in water photocatalysis reactions. Heat treating sample at 800 °C proved to be beneficial to the photocatalytic activity. Besides reducing the samples' bandgap, the heat treatment also increased the concentration of O_2 vacancies in these materials.$TiO_2/Na_2WO_4.2H_2O$ samples showed the highest photocatalytic capacity to produce H_2 and absorb visible light. The probable reason for this is the hydroxyl groups and Na's presence in the sample's surface. Nonetheless, the use of tungsten doping imprisoned the electrons by physically separating the semiconductor charges, thus increasing the electron lifespan and preventing the recombination of electron/hole pairs.

Declaration of competing interest

The authors declare no conflict of interest.

Acknowledgments

The authors would like to thank the support provided by Conselho Nacional de Desenvolvimento Científico e Tecnológico (CNPq), Coordenação de Aperfeiçoamento de Pessoal de Nível Superior (CAPES), Fundação de Amparo à Pesquisa do Estado do Rio Grande do Sul (FAPERGS) and Universidade Federal do Rio Grande do Sul (UFRGS).

References

Bharti, B., Kumar, S., Lee, H.N., Kumar, R., 2016. Formation of oxygen vacancies and Ti^{3+} state in TiO_2 thin film and enhanced optical properties by air plasma treatment. Sci. Rep. 1–12. https://doi: 10.1038/srep32355.

Chou, L.Y., He, R.L.W., Geh, N., Lin, Y., Hou, E.Y.F., Wang, D., Hou, H.J.M., 2012. Direct oxygen and hydrogen production by water splitting using a robust bioinspired manganese-oxo oligomer complex/tungsten oxide catalytic system. Int. J. Hydrogen Energy 37, 8889–8896. https://doi.org/10.1016/j.ijhydene.2012.02.074.

El-Yazeed, A.W.S., Ahmed, A.I., 2019. Photocatalytic activity of mesoporous WO_3/TiO_2 nanocomposites for the photodegradation of methylene blue. Inorg. Chem. Commun. 105, 102–111. https://doi.org/10.1016/j.inoche.2019.04.034.

Empresa de Pesquisa Energética, 2020. Atlas da Eficiência Energética, Relatório de Indicadores, Brasil. http://www.epe.gov.br/pt/abcdenergia/matriz-energetica-eeletrica#ENERGETICA (acesso em 11 de fevereiro de 2020.

Garcia, A.P., Guaglianoni, W.C., Garcia, D.R., Soares, L.G., Vaz, M.O., Teixeira, S.R., Pereira, M.B., Basegio, T.M., Clemens, F.J., Alves, A.K., Rodembusch, F.S., Bergmann, C.P., 2018. Facile synthesis by peroxide method and microwave-assisted hydrothermal treatment of TiO_2 with high photocatalytic efficiency for dye degradation and hydrogen production. Chem. Sel. 3, 11454–11459. https://doi.org/10.1002/slct.201802188.

Hao, L., Miyazawa, K., Yoshida, H., Lu, Y., 2018. Visible-light-driven oxygen vacancies and Ti^{3+} co-doped TiO_2 coatings prepared by mechanical coating and carbon reduction. Mater. Res. Bull. 97, 13–18. https://doi.org/10.1016/j.materresbull.2017.08.023.

Kingery, W.D., Bowen, H.K., Uhlmann, D.R., 1976. Introduction to Ceramics, 2ª. Edição. Wiley-Interscience.

Li, W., Body, M., Legein, C., Dambournet, D., 2017. Identify OH groups in $TiOF_2$ and their impact on the lithium intercalation properties. J. Solid State Chem. 246, 13–118. https://doi.org/10.1016/j.jssc.2016.11.010.

Liu, R., Lin, Y., Chou, L.Y., Sheehan, S.W., Wanshu, H., Zhang, F., Hou, H.J.M., Wang, D., 2011. Water splitting by tungsten oxide prepared by atomic layer deposition and decorated with an oxygen-evolving catalyst. Angew. Chem. Int. Ed. 50, 499–502. https://doi.org/10.1002/anie.201004801.

Marques, F., Stumbo, A.M., Canela, M.C., 2017. Estratégias e materiais utilizados em fotocatálise heterogênea para geração de hidrogênio através da fotólise da água. Quim. No. 40, 561–571. https://doi.org/10.21577/0100-4042.20170015.

Muccillo, E.N.S., 2008. Condutores de íons oxigênio - uma breve revisão. Cerâm. 54, 129–144. https://doi.org/10.1590/S0366-69132008000200002.

Nguyen, T.A., Tae-Sun, R., Muhammad, R., Shin, K.Y., 2011. Synthesis of mesoporous tungsten oxide nanofibers using the electrospinning method. Mat. Lett. 65, 2823–2825. https://doi.org/10.1016/j.matlet.2011.05.103.

Oliveira, M.V., 2016. Síntese caracterização de nanotubos de óxidos e oxinitretos de tântalo para geração de hidrogênio através fotólise da água. 78p. Dissertação (Mestrado em Ciência dos Materiais) – Programa de Pós-Graduação em Ciência dos Materiais. PGCIMAT/RS, Porto Alegre.

Patsoura, A., Kondarides, D.I., Verykios, X.E., 2006. Enhancement of photoinduced hydrogen production from irradiated Pt/TiO2 suspensions with simultaneous degradation of azo-dyes. Appl. Catal. B. 64, 171–179. https://doi.org/10.1016/j.apcatb.2005.11.015.

Patsoura, A., Kondarides, D.I., Verykios, X.E., 2007. Photocatalytic degradation of organic pollutants with simultaneous production of hydrogen. Catal. Tod. 124, 94–102. https://doi.org/10.1016/j.cattod.2007.03.028.

Prabhu, S., Nithya, A., Mohan, S.C., Jothivenkatachalam, K., 2014. Synthesis, surface acidity and photocatalytic activity of WO_3/TiO_2 nanocomposites – an overview. Mater. Sci. For. 63–78. https://doi.org/10.4028/www.scientific.net/MSF.781.63.

Rifkin, J., 2003. A Economia do Hidrogênio. Books, São Paulo.

Sato, S., White, J.M., 1980. Photodecomposition of water over Pt/TiO_2 catalysts. Chem. Phys. Lett. 72, 83–86. https://doi.org/10.1016/0009-2614(80)80246-6.

Soares, L.G., Alves, A.K., 2018. Photocatalytic properties of TiO_2 and TiO_2/WO_3 films applied as semiconductors in heterogeneous photocatalysis. Mat. Lett. 211, 339–342. https://doi.org/10.1016/j.matlet.2017.10.023.

Tan, Y., Shu, Z., Zhou, J., Lib, T., Wang, W., Zhao, Z., 2018. One-step synthesis of nanostructured $g\text{-}C_3N_4/TiO_2$ composite for highly enhanced visible-light photocatalytic H_2 evolution. Appl. Catal. B Environ. 230, 260–268. https://doi.org/10.1016/j.apcatb.2018.02.056.

Tolmasquim, M.T., 2003. Fontes Renováveis de Energia no Brasil, primeira ed. Interciência, Brasil.

Vasconcelos de Sá, L.R., Cammarota, M.C., Leitão, V.S.F., 2014. Produção de hidrogênio via fermentação anaeróbia – aspectos gerais e possibilidade de utilização de resíduos agroindustriais brasileiros. Quim. No. 37, 857–867. https://doi.org/10.5935/0100-4042.20140138.